UNIVERSITY^{OF} BIRMINGHAM

Roller compaction

Mahmah, Osama ; Adams, Michael; Omar, Chalak ; Gururajan, Bindhu ; Salman, Agba

Document Version
Peer reviewed version

[Link to publication on Research at Birmingham portal](#)

Article

Roller compaction: Ribbon splitting and sticking

Osama Mahmah[1], M.J. Adams[2], Chalak S.Omar[1], Bindhu Gururajan[3] & Agba D. Salman[1]

[1] Department of Chemical and Biological Engineering, University of Sheffield, Sheffield, S1 3JD, UK;

   omahmah1@sheffield.ac.uk

[2] School of Chemical Engineering, University of Birmingham, Edgbaston, Birmingham, B15 2TT, UK;

   M.J.Adams@bham.ac.uk

[3] Novartis Pharma AG, 4057 Klybeckstrasse, Basel, Switzerland

* Correspondence: omahmah1@sheffield.ac.uk; Tel.: +44 (0)114 222 7543

Abstract:

Roller compaction is the main technique employed in dry granulation. Ribbon sticking and splitting are among the major factors that can hinder the use of this process for some formulations. Ribbon splitting can occur either transversally (through the ribbon thickness) or longitudinally (through the ribbon width). It was observed that transverse splitting is commonly associated with sticking of the split ribbons to the rollers and results in an inferior performance of the process. Longitudinal splitting is associated with an across-width distribution of the ribbon density so that there may an adverse effect on the mechanical strength and dissolution properties of the tablets formed from the milled granules. The aim of the current work was to elucidate the mechanisms of splitting by an experimental study involving single component powders with a range of yield strengths, including those that are commonly used as excipients. Both smooth and knurled rollers were employed without and with lubrication by applying magnesium stearate to the rollers. The minimum gap was fixed and the maximum roll stress was varied. The observed trends for the smooth rollers were rationalised in terms of a splitting index, which is a measure of the residual stresses driving crack growth relative to the tensile strength of the ribbons. There was a lower limit at which splitting was observed but the occurrence of transverse splitting decreased and that for longitudinal splitting increased with increasing values of the index, which was accompanied by an increase in mixed transverse-

longitudinal splitting. Transverse splitting was always associated with sticking to the rollers and was prevented by external lubrication. The main difference with the knurled rollers was that in some cases transverse splitting occurred without sticking to the rollers. A detailed discussion of the mechanisms involved is presented.

1. Introduction

Roller compaction is a pressure mediated dry granulation process by which materials are agglomerated without a liquid binder. A powder is fed between two counter-rotating rollers by gravity from either a hopper or a screw feeder. Initially, the powder slips against the rollers but eventually the increase in the wall shear stress is sufficient to prevent such wall slip; this occurs at the so-called nip angle, which is the downstream angular difference relative to that at the minimum gap between the rollers. In this compaction zone, high stresses are applied to produce a ribbon, which is subsequently milled into granules of a specified particle size range (Kleinebudde, 2004; Omar et al., 2015).

Despite roller compaction being well established, there remain intrinsic challenges to ensuring that the design and operation is sufficiently optimal. Leakage of relatively high amounts of uncompacted powder between the seals of the rollers can greatly affect the process efficiency. The heterogeneity of the ribbons in terms of the density distribution across the width has a negative impact on the uniformity of downstream granules (Gamble et al., 2010; Guigon and Simon, 2003). Ribbon-roller adhesion can also cause serious difficulties. Hamdan et al. (Hamdan et al., 2010) observed that variations in the roll gap, and hence ribbon density, could be attributed to such adhesion. Dawes et al. (Dawes et al., 2012a), concluded that the sticking of an adhesive powder formulation can be inhibited by external lubrication of the rollers using magnesium stearate (MgSt). They also investigated the effects of internal lubrication by incorporating MgSt in the powder feed. It was observed that without MgSt, sticking occurred 30-60 s after start up and was more problematic when operating in the automated roll gap control mode, which controls the set gap by adjusting the speed of the screw feeder. The extent to which the speed of the auger changes, and hence the mass throughput, depends on the thickness of the adhered layer (Dawes et al., 2012b). However, ribbons did not stick when MgSt was added to the formulation. When the powder adheres to the rollers, it disturbs the integrity of the ribbon and so affecting the continuity of the process.

There are a considerable number of studies that have investigated the phenomenon of powder-metal adhesion in the field of tabletting. The adhesion to the punches is mainly attributed to either the formulation or the process conditions. Hygroscopicity, cohesiveness, low melting point, insufficient lubrication and/or unsuitable powder characteristics such as particle size and polymorphism are the main formulation based factors (Lam and Newton, 1991; Paul et al., 2017; Podczeck et al., 1996). The use of an unsuitable surface configuration, excessively small compaction pressures, and/or rough surfaces are the main process based causes (Saniocki, 2014). However, sticking to a roller surface has not been investigated in detail where a different combination of shear and normal stress are involved.

Ribbon splitting is one of the main problems (Osborne, 2013), which has the potential to occur in different directions because of the complexity of the stress field imposed on the powder feed. Guigon et al. (Guigon et al., 1996) observed different types of ribbon splitting as one of the common defects that could occur when using fine powders. Wu et al. (Wu et al., 2010) investigated the effects of the moisture content of microcrystalline cellulose (MCC) as a feed powder, and noted that the ribbons produced at high values (>11.44 %) tended to split across the width. It was ascribed to the resulting reduction in the tensile strength of the ribbons. Ende et al. (Ende et al., 2007) reported that, for a range of powder feeds, the occurrence of ribbon splitting (the exact location of the splitting was not mentioned) was minimised when the gap was < 2.6 mm. Cunningham et al. (Cunningham et al., 2010) suggested that the reversal of the direction of the shear stress at the neutral angle could be a contributory factor given that particle compacts are weak in shear. However, it would be difficult to evaluate experimentally. Ribbon splitting is analogous to the capping and lamination phenomena observed in a tabletting process, which is ascribed in the literature to various process and formulation parameters (Hiestandx et al., 1977; Paul and Sun, 2017; Wu et al., 2008). Critical factors are the stored elastic strains, non-uniform density distribution, sticking to the punches and air entrainment.

Thus, previous research has focussed mainly on the consequences of ribbon splitting and some of the mitigation approaches. The aim of the current work was improve the mechanistic understanding of this phenomenon in terms of the ribbon-roller interactions in both the bulk and at the roller walls. Feed powders with a range of yield strengths were roller compacted and the nature of the cracks in the ribbons was observed with and without MgSt applied directly to the rollers. Depending on the applied

pressure of the rollers, there were two types of cracks that occurred in isolation or in combination: through-width and through-thickness, which will be referred to as *longitudinal* and *transverse cracks*. It was possible rationalise this behaviour by measurement of the density distribution across the ribbons, their tensile strength and their adhesion to the rollers.

2.1 Feed powders

The excipients were selected to produce a gradual change in the mechanical properties, i.e. mechanical properties that ranged from $CaCO_3$ as hard particles and a high yield strength value to a more plastically deformable particles of MCC. Seven different powders with a range of mechanical properties were selected: calcium carbonate ($CaCO_3$) (Longcliffe Quarries Ltd., UK), maltodextrin (Glucidex 6, Roquette, France), α-lactose monohydrate 200M (GranuLac® 200, MEGGLE Germany), microcrystalline cellulose (MCC) (VIVAPUR®101, JRS PHARMA, Germany), anhydrous lactose (NF-DT, Kerry bioscience, USA), mannitol C160 (Pearltol®C160, Roquette, France), and pregelatinized maize starch (Starch 1500®, Colorcon, UK). The effects of externally lubricating the rollers were investigated by applying 0.25 g magnesium stearate (MgSt) (Peter-Greven). Scanning electron micrographs of the particles are shown in Figure A1.

The powders were equilibrated for three days at a relative humidity of 40% and a temperature of 25°C in an environmental chamber (Binder KMF 240 climatic chamber, Binder, UK). Their particle size distributions were measured using a Camsizer XT (Retsch Technology GmbH, Germany) as shown in Table 1 together with their true densities as supplied by the manufacturer.

2.2 Methods

2.2.1 Powder characterization

2.2.1.1 Yield strength and elastic recovery

The yield strengths of the particles were estimated by analysing confined uniaxial compaction data using the Heckel equation, which is based on the compact density as a function of the applied force (Heckel, 1961). Although it involves a number of limitations (Sonnergaard, 1999), it is still used extensively as a valuable tool for comparing the mechanical properties of powders. A sample of 0.4 g of a powder was added to a 12 mm diameter polished stainless steel die and compressed at a speed of 1 mm/min using a universal testing machine (Instron 3367, USA) for a range of maximum compaction forces (1, 3, 5, 10, and 15 kN corresponding to roll pressures of 8 - 176 MPa). The loading and unloading energies were also calculated from the force-displacement data. The elastic recovery, $\varepsilon_R(\sigma_{max}, K)$, was calculated using the following expression:

$$\varepsilon_R(\sigma_{max}, K) = \varepsilon_U/\varepsilon_L \tag{1}$$

where $\varepsilon_R(\sigma_{max}, K)$ is a function of the maximum roll stress, σ_{max} (MPa), and the yield strength, K (MPa), and ε_L and ε_U are the loading and unloading energies (J) such that $\varepsilon_R = 0$ corresponds to perfectly plastic deformation and $\varepsilon_R = 1$ to perfectly elastic deformation.

2.2.1.2 Maximum roll stress determination

In order to calculate the maximum roll stress acting on the feed powders, a ring-shear cell tester RST-XS.s (Dr. Dietmar Schulze, Germany) was employed to measure both the effective angle of internal friction, δ_E, and angle of wall friction, $\emptyset_w$. To measure δ_E, the powder was pre-consolidated by applying a specified normal load and pre-sheared until steady state was reached. Subsequently, shearing was applied under reduced normal loading steps. A stress of 5 kPa was applied as a pre-shear normal stress and three different normal stresses of 1.50, 2.75, and 4.00 kPa were applied sequentially. The measurement of $\emptyset_w$ was based on determining the sliding resistance between the powder and a metal surface at different applied normal forces with 5 kPa as a pre-shear. This involved using a smooth stainless steel coupon (surface roughness Ra ~ 2.44 ± 0.3 μm) and a knurled stainless steel coupon (stainless steel 4140, Ra = 108.6 ± 4.37 μm), which have similar surface finishing to the rollers. The knurled coupon was machined using wire-electrical discharge machine (EDM) to have the same diagonal cross hatch cuts as the knurled rollers. Optical images of the sections of the rollers are shown in Figure 1.

The maximum applied roll stress and nip angle were calculated using the analysis developed by Johanson (Johanson, 1965), which has been employed by many researchers (Bindhumadhavan et al., 2005; Yusof et al., 2005). To calculate the nip angle for the knurled rollers, the total depth of the surface topographical valleys was set to 1 mm. Recent work has shown that one limitation of the approach is the application of a power law relationship between the stress and the ribbon density since it does not capture the behaviour at small pressures (Patel et al., 2010). Consequently, the uniaxial compaction data was fitted to an alternative relationship developed by Adams et al. (Adams et al., 1994) that was adopted in (Patel et al., 2010).

2.2.2   Roller compaction

2.2.2.1   Roller compaction system and ribbon production

The roller compactor was an Alexanderwerk WP120 (Alexanderwerk, Germany), which incorporates a feeding, compaction, and milling system and is equipped with a de-aeration system that can enhance the powder flowability and play a role in reducing the amount of fines. The counter-rotating rollers have widths of 4 cm and diameters of 12 cm. The feeding system is a horizontal auger and the rotational speed and, hence the applied pressure, can be varied. The gap between the two rollers is sealed with two side cheek plates that are designed to prevent powder leakage during compaction. They are fabricated from Teflon and have a surface roughness Ra of 3.57 ± 0.82 μm. Metallic scrapers are fixed at about 0.1 mm distance from the roller surfaces. There is a gap feedback system that controls the screw feeder speed in order to deliver the powder flow rate that will maintain the required gap between the rollers. The relationship between roller separating force and hydraulic pressure is given by the manufacturer (Alexanderwerk) (Al-Asady et al., 2015) and tabulated in the Appendix (Table A1).

To examine the effects of the surface topography of the rollers, two pairs of rollers with different surfaces (knurled and smooth) were used in this study. The indentation depth of the knurled roller is about 0.5 mm, which was measured with a digital microscope (Keyence VHX-5000). It was also used to measure the surface roughness (Ra values) of the roller surfaces, which is about 2.6 ± 0.2 μm for the smooth rollers and 119.4 ± 5.9 μm for the knurled rollers.

The conditioned powder was compacted at different hydraulic pressures in the range 1.8 - 23 MPa. A fixed roller gap of 2 mm and a fixed roller speed of 3 rpm were employed. In order to investigate the effects of adhesion between the ribbons and rollers, 0.25g of MgSt as a lubricant was applied to each

roller surface using a brush. The ribbons were only collected after a steady state hydraulic pressure and roller gap was achieved.

2.2.2.2 Uncompacted fines

The entire product (ribbons and fines) were collected for a set period of time. The amount of fines arising from uncompacted powder is defined as particles that are smaller than the d90 of the original powder. The ribbons were separated from the fines by sieving (Retsch GmbH, Germany) and the mesh size was selected according to the d90 of the used powder. The mass of the entire product was weighed together with that of the mass of separated fines to calculate the weight percentage of the fines.

2.2.2.3 Roller-powder adhesion

To estimate the strength of adhesion of the powder feed to the rollers, the particulate debris after one of the scrapers was recorded using a high-speed camera (Photron Fastcam 1024 PCI, Itronx Imaging Technologies, CA) that was set to capture 60 fps with a recording area of 30 x 40 mm. Seven minutes of videos were recorded for all powder feeds with the smooth rollers. Given that the roller speed was 3 rpm, this is equivalent to ~ 25200 images from which only the first roller cycle (1200 images) were processed using Image J software (National Institutes of Health (NIH), USA). This software uses a grey scale system that ranges from 0 to 255; where zero is complete black and 255 is complete white. An image of the roller surface was used to identify the grey value of the roller without any powder debris; any grey value greater than this threshold was considered as adhered powder. Subsequently, the software was used to quantify the fraction of white pixels, which corresponds to that of the powder particles.

2.2.3 Ribbon characterization

2.2.3.1 Ribbon tensile strength

The tensile strength of the ribbons formed from the smooth rollers were measured using a three-point bend configuration. This involves two lower supports for the ribbon and a sharp metal plate that is attached to a Zwick/Roell Z 0.5 (Zwick/Roell, Germany) universal test machine. The test machine applies the load at the centre of the ribbon at a rate of 1 mm/min. The tensile strength was calculated using the following expression:

$$\sigma_{\mathrm{T}} = \frac{3F_{\max}L}{2bd^2} \tag{2}$$

where σ_{T} is the tensile strength (MPa), $F_{\max}$ is the maximum loading force corresponding to crack initiation (N), b and d are the width and thickness of the ribbon (mm), L is the distance between the two supports (mm), which was set depending on the ribbon thickness according to the British standards (L= (16 ± 1) d) (Omar et al., 2015; Standard institution, 1977) . The measurement procedure was repeated at least ten times for the ribbons produced under each condition.

2.2.3.2   Ribbon solid fraction

The solid fraction across the ribbon widths was measured using X-ray microtomography (microCT 35, Scanco Medical AG, Switzerland). The X-ray was operated at a voltage of 45 KV, a power of 8 W, and a current of 177 μA.

Reconstructed images were processed using Image J software (National Institutes of Health (NIH), USA). The grey value of the air was determined using the histogram of the specified area in the air surrounding the ribbon sample, which was used to identify air within the ribbon sample. Any grey value below this was considered as air and above this as solid sample (ribbon).

The ratio of air to ribbon pixels is a measure of the porosity of the selected sample area. The scanning was conducted on non-split ribbons and, where necessary, on longitudinally split ribbons. The measurements were performed at increments of 3.5 mm across the ribbon width.

The relative difference in the solid fraction,$\Delta\beta$, is defined by the following relationship:

$$\Delta\beta = (\beta_C - \beta_E)/\beta_C \qquad\qquad\qquad (3)$$

where β_C is the minimum solid fraction across the ribbon width and β_E are the solid fractions at about 1 mm from the ribbon edge.

3. Results

The fitting of the die compaction data to the Heckel (Heckel, 1961) and Adams et al. (Adams et al., 1994) equations together with the values of the fitting parameters (yield strength and compressibility factor) are given in Tables 1 and 2 respectively.

The elastic recoveries as a function of the yield strength for the different hydraulic pressures are shown in Figure 2. For all feed powders, the elastic recovery increases with increasing hydraulic pressure. There is also small but not systematic increase with increasing yield strength.

The maximum roll stress as a function of the hydraulic pressure for the unlubricated smooth and knurled rollers calculated using the measured powder properties are shown in Figure 3. They exhibit a linear relationship with the gradients for a given feed powder being greater for the smooth rollers since the nip angles are less (Figure 4), i.e. the contact area with the rollers is smaller at a given roll force as defined by the set hydraulic pressure. That is, the knurled rollers will change both the angle of wall friction and depth of indentation. However, the minimum gap is maintained at a constant value so that the trend of maximum stress will change according to the sensitivity of the material to a change in the wall friction for both types of rollers. For example, using knurled rollers has changed the angle of wall friction of mannitol by a factor of about three while the corresponding change for CaCO3 is only two.

To first order, the tensile strength of the ribbons formed with the smooth rollers increased linearly with increasing maximum roll stress and the mean ratio increases with increasing values of the reciprocal of the yield strength (Figure 5). The anomalous behaviour of starch in this figure and Figure 2 can probably be ascribed to the viscoelasticity of this material. Starch is reported to be more sensitive

to the dwell time than the other powders used in this study, (Al Asady et al., 2018; Chang et al., 2008). (Al Asady et al., 2018) has investigated the effects of compaction speed on a similar set of materials to those used in the current study (including $CaCO_3$, lactose 200M, MCC, starch and maltodextrine). They observed that starch has a relatively high dependency on the compaction speed, i.e, unlike the other powders, as reflected in the strength of the compacts.

The line in Figure 5 is the best linear fit to the data (R^2 = 0.94) and corresponds to the following expression, where the intercept represents the minimum yield strength required to form a coherent ribbon:

$$\frac{\sigma_T}{\sigma_{max}} = 2.90K^{-1} - 0.01 \tag{4}$$

MCC powder forms the strongest ribbons while $CaCO_3$ powder forms very weak ribbons. The ribbons for all the powder feeds exhibited unstable fractures except for $CaCO_3$ (Figure 6).

The ribbons made with knurled rollers exhibited similar trends but were considerably weaker. It was difficult to measure the ribbon thickness accurately due to the presence of knurling patterns on the ribbons, which increased the uncertainty and variability of the data. However, the results demonstrated that these ribbons were considerably weaker, which may be ascribed to the greater porosity at a similar maximum roll stress as exemplified by the X-ray images in Figure 7; there is a greater number density of black pixels (air) for the ribbon with the knurled rollers. The porosity profiles for all ribbons made with knrled and smooth rollers are shown in Figure A2.

Table 3 summarises the effects of the hydraulic pressure on the sticking and splitting behaviour of the different powder feeds in descending order of their single particle yield strengths for the unlubricated smooth and knurled rollers. Sticking refers to the physical adhesion of the ribbon to the two rollers and it is always associated with transverse splitting. The transversal (through-thickness) and longitudinal (through-width) splitting are classified as 'T' and 'L' respectively. Shaded areas in red indicate the occurrence of the splitting or sticking. Shaded areas in green correspond to conditions under which splitting or sticking does not occur. As exemplified in Figure 8 for Mannitol C160

ribbons, there are transitions in the longitudinal splitting behaviour with increasing applied stress from the ribbon being coherent to splitting into two ('L2') and three ('L3') sections and also splitting from the edge so that the cracks are joined ('LJ'). However, increasing the applied stress (≥122 MPa) for maltodextrin, resulted in an increase in the ribbon temperature to a value that is greater than the glass transition temperature of this material (80°C) (Castro et al., 2016), which resulted in the ribbons adhering to the roller surface and splitting transversally.

The application of MgSt to the smooth knurled rollers completely inhibited sticking and transverse splitting but similar longitudinal splitting was observed. The unlubricated knurled rollers showed a similar transversal splitting trend to that of the smooth rollers except that the more plastically deformable powder feeds exhibited such splitting up to greater maximum roll stresses. However, they reduced the occurrence of longitudinal splitting compared to the unlubricated smooth rollers. It was also observed that avoiding transversal splitting/roller sticking by increasing the applied stress was associated with a significant reduction in the amount of fines. The percentage of fines decreased with increasing roll stress and approximately with decreasing values of the single particle yield stress as shown for the unlubricated smooth rollers in Figure 9. The trends correspond to a reduction in the occurrence of transversal splitting. The relative difference in the solid fraction across the width of the ribbons as a function of the maximum roll stress is shown in Figure 10 for the smooth and knurled rollers except for $CaCO_3$ since the ribbons were too weak for the measurement procedure. It was clear that the relative differences across the widths of the ribbons was less than for the corresponding ribbons formed with the smooth rollers.

The particle debris coverage on the smooth rollers after the scrapers as a function of the maximum roll stress for the powders that exhibited adhesion is shown in Figure 11. The extent of the coverage reduces with increasing roll stress and asymptotically approaches zero. The coverage for starch, MCC and $CaCO_3$ was approximately zero, which was also the case for matodextrin until it melted.

4. Discussion

In the exit region of the rollers, corresponding to upstream angles greater than that the minimum gap, a ribbon will undergo elastic recovery. If the residual stresses are greater than the critical fracture stress, ribbon splitting may be initiated. Moreover, if there is adhesion to the rollers, the resulting bonding stresses will augment the residual stresses; this may be the case even when there is not visible particle debris on the surfaces of the rollers since adhesive rather than cohesive failure may still impose small opening stresses. For the smooth rollers (Table 3(a)), with the exception of the $CaCO_3$ ribbons, transverse splitting only occurs when there is sticking to the rollers and thus only longitudinal splitting is possible when the rollers are lubricated. Ribbons made from $CaCO_3$ are the exception in exhibiting transvers splitting even though sticking to the rollers does not occur. However, for the knurled rollers (Table 3(b)), transverse splitting was observed for some powders despite sticking being absent.

It is evident from Table 3 that the combined influence of the maximum roll stress and the yield strength are critical factors in ribbon splitting. This is more directly clear in the case of pure longitudinal splitting i.e. also excluding mixed longitudinal-transverse splitting. Figure. 12 maps the transition from no splitting to longitudinal splitting in coordinates of the maximum roll stress and the yield strength for the unlubricated and externally lubricated smooth rollers, for which the results were identical i.e. this includes mixed splitting outcomes that revert to pure longitudinal splitting. It shows that there is a lower limit of the maximum roll stress above which, depending on the yield strength, longitudinal splitting occurs. For a yield strength greater than ~ 130 MPa, the critical roll stress at which such splitting occurs reduces considerably. The sensitivity of longitudinal splitting to increasing the roll stress and the yield strength is clearly related to the increase in the elastic recovery (Figure 2).

The compaction of powder assemblies is accommodated by a combination of number of mechanisms that may include the rearrangement, elastic or elastoplastic deformation and fracture of the particles. It is well established that the stress is not transmitted uniformly but through force chains that increase in number density with increasing stress. Thus, as particles become progressively subjected to increasing stress, it will eventually cause them to deform plastically rather elastically when their yield strength is exceeded, and thus reducing the contribution to the elastic recovery. This would also be the case for particle rearrangement and

fracture. Moreover, greater yield strengths are associated with less cohesion of the compacted particles so that the tensile strength of the ribbons decreases with increasing values of the yield strength (Figure 5). Another parameter that could contribute to the explanation of the trend found in the association between tensile strength and deformability (Figure 5) is the crystallinity. An increasing amorphous content is expected to enhance the molecular mobility and deformability during stress application, which could be reflected in a stronger compact. Such behaviour was reported in (KOPP et al., 1989) who studied a similar set of materials as in this study. $CaCO_3$ and mannitol are pure crystalline materials with very limited deformability as expected from their yield strength values. MCC, maltodextrin and starch have a higher amorphous contents and exhibited greater deformabilities and consequently stronger ribbons (Figure 5 and Table 1). However, the improvement in compaction behaviour can be due to several factors in addition to the amorphous content e.g. particle size and shape could also change the particle deformability (Hancock et al., 2002; Omar et al., 2015); this could explain the non-systematic trend if the powders are ordered only according to their amorphous content and yield strength.

A critical factor in longitudinal splitting is the relative difference in the solid fraction across the ribbons (Figure 10) since it is related to the variation in the elastic recovery. To understand the origin of the relative difference in the solid fraction, which has been observed previously (Miguélez-Morán et al., 2009), it is useful to consider roller compaction as a combination of shear and squeeze flow. The squeeze flow component exerts back-pressure upstream resulting in the maximum pressure occurring at an angle that is greater than that corresponding to the minimum gap, which is normally taken as zero. This angle is approximately equal to the neutral angle at which the shear stress is zero due to its change of direction (Cunningham et al., 2010). More importantly, the squeeze component results in a lateral pressure distribution that has a maximum value in the centre of the width of the ribbon. Such non-uniform pressure distributions are observed in the compression of all fluids, solids, and granular systems e.g. metals (Johnson and Mellor, 1973) and pastes (Adams et al., 1997). They arise from the resistance to deformation/flow caused by no slip or friction at the contacting walls. As a result, the powder feed in a roller compactor is more compressed in the centre of the ribbon compared to the edges

as demonstrated in the current measurements of the relative difference in the solid fraction across the ribbons (Figure 10). This has important implications for ribbon splitting as discussed below.

Since the solid fraction is greater in the centre of a ribbon, the maximum roll stress must be greater in this region compared to the edges. Thus in the exit region, the stored elastic strain, and hence the expansion of the ribbon, will greatest in the centre of a ribbon. Consequently, bending stresses are developed that increase from zero in the centre of the thickness to a maximum value on the surfaces. As a result, longitudinal splitting always occurs in the centre of the width of the ribbons where the crack opening stresses will be greatest. The importance of the lateral pressure distribution is reflected in the reduced occurrence of longitudinal splitting for ribbons formed from the knurled rollers for which the relative difference in the solid fractions across the width of the ribbons is less (Figure 10).

Given the importance of the maximum roll stress and the yield strength in longitudinal splitting, the ratio is a useful dimensionless quantity for quantifying the ranges under which no splitting and longitudinal splitting occur. This is shown in Figure 13(a) for the unlubricated and lubricated smooth rollers as a histogram based on the outcomes per powder type normalised by the total number of outcomes. As this ratio increases in value, there is a general reduction in the number of no splitting outcomes and an increase in those for longitudinal splitting. However, both outcomes are evident for the whole range so that this ratio only provides an indication of the change in the probability of no splitting.

An alternative dimensionless quantity is a splitting index, I_S:

$$I_S = \varepsilon_R \sigma_{max}/\sigma_T \qquad (5)$$

which is analogous to the capping index proposed for tabletting (Akseli et al., 2013). It is more fundamental in terms of its mechanistic interpretation than the ratio σ_{max}/σ_Y but requires that roller compaction has to be carried out in order to measure σ_T before it can be employed for assessing formulations and operating conditions. As before, it leads to a trend of decreasing no splitting and

increasing longitudinal splitting as the values of this parameter increases (Figure 13(b)). However, there is an upper limit at which splitting always occurs. That the values increase to ~ 45 rather than the ideal case of the critical condition for splitting being approximately unity arises because the numerator in Eq. (5) is some measure of the residual stress acting vertically rather than the actual crack opening stresses acting at the two surfaces of a ribbon.

Despite having the largest yield strength, and hence the highest elastic recovery and weakest ribbons, $CaCO_3$ ribbons never split longitudinal. The probable cause is that the ribbons exhibit stable fracture unlike those formed by the other powder feeds (Figure 6). A characteristic of stable fractures is that crack propagation is arrested when the driving force or displacement ceases; a common example is tearing paper. Thus, it may be assumed that the stored elastic strains in $CaCO_3$ ribbons are less than the critical value required to significantly propagate a longitudinal crack. In the case of the ribbons made from the other powders, the instability of the crack growth will result in catastrophic crack propagating once it is initiated. It is more difficult to understand the factors that result in the $CaCO_3$ ribbons splitting transversely in the absence of observable adhesion to the rollers. As mentioned previously, it has been argued, on the basis of finite element modelling, that the reversal of the shear stress and strain at the neutral angle may result in fracture/lamination since pharmaceutical powder compacts are generally weak under shear (Cunningham et al., 2010). That is, weak adhesion forces to the rollers may be sufficient to cause such a weak plane to fracture transversely. The $CaCO_3$ ribbons would be particularly susceptible to such a mechanism since they are so mechanically weak in any case.

For the smooth rollers with the exception of $CaCO_3$, transverse splitting and also mixed transverse-longitudinal splitting is always associated with sticking of the spilt ribbons to the rollers (Table 3). This has two effects: (a) the adhesive forces acting on a ribbon prevent bending strains being developed as would be the case for a ribbon that was not adhered to the rollers and (b) the adhesive forces coupled with the residual stresses result in an increased crack opening stress across the width of a ribbon approximately in the centre of the thickness. A histogram involving the splitting index for the unlubricated smooth rollers that includes transverse and mixed splitting is presented in Figure 14.

There is a lower limit at which no splitting occurs after which pure transverse splitting is prevalent but decreases until there is a transition to mixed and longitudinal splitting. While the index is a useful means of categorising the data for transverse and mixed splitting, it is of less fundamental value since it ignores the adhesive stresses acting on the ribbons.

For smooth rollers, longitudinal splitting was initiated at a value of the splitting index in the range 0.9-4.27 while for knurled rollers, it was 13.8-24.5. This may be due to the index not fully taking account of the bending stresses. In an attempt to improve the generalisation of this index, it was modified by incorporating the relative solid fraction difference since the bending stresses should scale with parameter. The modified splitting index, I_S', is defined as follows:

$$I_S' = \Delta \beta \varepsilon_R \sigma_{max} / \sigma_T \tag{6}$$

and the data Figure 14 have been replotted in Figure A3 in terms of this index. The advantage of this index is that the values that correspond to the initiation of longitudinal splitting are more similar for the smooth (1.6 – 3.2) and knurled (1.6 – 7.11) compared with those for the unmodified index, which had values of (1.0 – 4.2) and (13.8 – 24.6). That is, this index can be generalized to both types of rollers.

There are some similarities with the splitting behaviour associated with the knurled rollers (Table 3(b)), but transverse splitting is generally much more predominant except for maltodextrin within the limited pressure range at which melting does not occur. For example, starch and MCC exhibit only transverse splitting even though sticking to the rollers does not occur. The probable cause is the pressure distribution across the width of the ribbons is more uniform than for the smooth rollers as discussed previously (Figure 10). Consequently, the residual stress acting to split a ribbon transversely may be greater than that required for longitudinal splitting. In addition, the greater surface area of the knurled compared to the smooth ribbons may result in significant adhesive forces despite sticking not being observed as mentioned previously.

The use of single powder feeds has allowed the mechanisms of splitting and the critical factors that govern the occurrence of splitting to be established. However, in practice the feed powders are generally multi-component and include MgSt as an internal lubricant. Some limited studies were carried out to examine the effects of including 1 w/w% MgSt with mannitol C160, lactose 200M,

anhydrous lactose and $CaCO_3$ powders using the smooth rollers. The results were relatively similar to the feeds without MgSt except that sticking to the rollers did not occur and, for anhydrous lactose, there was no splitting up to hydraulic pressures of 80 bar whereas without MgSt splitting occurred at all pressures investigated.

The compression of practical formulations involving mixtures of powders is complex because it is likely to involve particles of different mechanical properties, shapes and size distributions. Systematic studies over a wide range of mixtures have not been reported for either roller compaction or tabletting although there is some evidence that simple mixture models could be applied (Frenning et al., 2009). In extending the current work to mixtures, measurements of the effective compressibility factor and yield strength by confined uniaxial compaction would be the most appropriate approach to adopt initially.

5. Conclusions

The splitting indices are useful parameters for understanding the fundamental factors that govern the occurrence of splitting. They are a measure of the stored elastic energy driving fracture relative to the fracture stress of the ribbons. The elastic recovery increases as the yield strength increases, which is associated with a reduction in the tensile strength of the ribbons. Thus, as demonstrated in Figures 14 and A3, an increase in splitting is promoted by large values of the yield strength. It is interesting that for the current feed powders, adhesion to the rollers reduced with decreasing values of the yield strength. For surface topographically rough monolithic solids, adhesion will exhibit the opposite trend since the stored elastic strains in the asperities, which act to resist adhesion, would be reduced by local elastoplastic deformation. For particle assemblies, a reduction in the yield strength increases the interparticle cohesive strength and thus reduces the probability of cohesive failure. However, this is not a monotonically increasing trend since eventually the reduction in the cohesive strength of the particles will become critical, which will eventually lead to splitting as observed by Wu et al., [9] who examined the effects of increasing moisture content on the roller compaction of MCC. Other detrimental

effects of excessively small yield strengths are a reduction in the flowability of the feed powder [9] and an increased probability of adhesion to the rollers and hence transverse splitting. The maximum roll stress increases the tensile strength of the ribbons and, consequently, plays an equivalent role to a reduction in the yield stress since it reduces the adhesion to the rollers. Thus increasing this stress leads to a transition from transverse to longitudinal splitting for the feed powders with the relatively large yield strengths. While longitudinal splitting does not prevent the ribbons from being milled, it is a result of a distribution of the ribbon density across the width. Consequently, it is not possible to make granules that all have optimal properties in terms of the mechanical strength and dissolution characteristics of the tablets. However, transverse splitting is generally associated with adhesion to the rollers that has a serious detrimental effect on the performance of the process.

Appendix

References

Adams, M.J., Aydin, I., Briscoe, B.J., Sinha, S.K., 1997. A finite element analysis of the squeeze flow of an elasto-viscoplastic paste material. J. Nonnewton. Fluid Mech. 71, 41–57. https://doi.org/10.1016/S0377-0257(96)01546-7

Adams, M.J., Mullier, M.A., Seville, J.P.K., 1994. Agglomerate strength measurement using a uniaxial confined compression test. Powder Technol. 78, 5–13. https://doi.org/10.1016/0032-5910(93)02777-8

Akseli, I., Ladyzhynsky, N., Katz, J., He, X., 2013. Development of predictive tools to assess capping tendency of tablet formulations. Powder Technol. 236, 139–148. https://doi.org/10.1016/j.powtec.2012.04.026

Al-Asady, R.B., Osborne, J.D., Hounslow, M.J., Salman, A.D., 2015. Roller compactor: The effect of mechanical properties of primary particles. Int. J. Pharm. 496, 124–136. https://doi.org/10.1016/j.ijpharm.2015.05.061

Al Asady, R.B., Hounslow, M.J., Salman, A.D., 2018. Roller compaction: the effect of plastic deformation of primary particles with wide range of mechanical properties. Drug Deliv. Transl. Res. 8, 1615–1634. https://doi.org/10.1007/s13346-018-0555-z

Bindhumadhavan, G., Seville, J.P.K., Adams, M.J., Greenwood, R.W., Fitzpatrick, S., 2005. Roll compaction of a pharmaceutical excipient: Experimental validation of rolling theory for granular solids. Chem. Eng. Sci. 60, 3891–3897. https://doi.org/10.1016/j.ces.2005.02.022

Castro, N., Durrieu, V., Raynaud, C., Rouilly, A., 2016. Influence of DE-value on the physicochemical properties of maltodextrin for melt extrusion processes. Carbohydr. Polym. 144, 464–473. https://doi.org/10.1016/j.carbpol.2016.03.004

Chang, C.K., Alvarez–Nunez, F.A., Rinella Jr., J. V., Magnusson, L.-E., Sueda, K., 2008. Roller Compaction, Granulation and Capsule Product Dissolution of Drug Formulations Containing a Lactose or Mannitol Filler, Starch, and Talc. AAPS PharmSciTech 9, 597–604. https://doi.org/10.1208/s12249-008-9088-y

Cunningham, J.C., Winstead, D., Zavaliangos, A., 2010. Understanding variation in roller compaction through finite element-based process modeling. Comput. Chem. Eng. 34, 1058–1071. https://doi.org/10.1016/j.compchemeng.2010.04.008

Dawes, J., Allenspach, C., Gamble, J.F., Greenwood, R., Robbins, P., Tobyn, M., 2012a. Application of external lubrication during the roller compaction of adhesive pharmaceutical formulations. Pharm. Dev. Technol. 18, 1–11. https://doi.org/10.3109/10837450.2012.705299

Dawes, J., Gamble, J.F., Greenwood, R., Robbins, P., Tobyn, M., 2012b. An investigation into the impact of magnesium stearate on powder feeding during roller compaction. Drug Dev. Ind. Pharm. 38, 111–22. https://doi.org/10.3109/03639045.2011.594802

Ende, M.T.A., Moses, S.K., Carella, A.J., Gadkari, R.A., Graul, T.W., Otano, A.L., Timpano, R.J., 2007. Improving the content uniformity of a low-dose tablet formulation through roller compaction optimization. Pharm. Dev. Technol. 12, 391–404. https://doi.org/10.1080/10837450701369253

Frenning, G., Nordström, J., Alderborn, G., 2009. Effective Kawakita parameters for binary mixtures. Powder Technol. 189, 270–275. https://doi.org/10.1016/j.powtec.2008.04.016

Gamble, J.F., Tobyn, M., Dennis, A.B., Shah, T., 2010. Roller compaction: Application of an in-gap ribbon porosity calculation for the optimization of downstream granule flow and compactability characteristics. Pharm. Dev. Technol. 15, 223–229. https://doi.org/10.3109/10837450903095342

Guigon, P., Simon, O., 2003. Roll press design - Influence of force feed systems on compaction. Powder Technol. 130, 41–48. https://doi.org/10.1016/S0032-5910(02)00223-1

Guigon, P., Simon, O., Saleh, K., Bindhumadhavan, G., Adams, M.J., Seville, J.P.K., 1996. Dry Granulation, in:

Salman, A.D., Hounslow, M.J., SevillE, J.P.K. (Eds.), Granulation. Elsevier, Amsterdam, pp. 255–286. https://doi.org/10.1016/S0022-3913(12)00047-9

Hamdan, I.M., Reklaitis, G. V., Venkatasubramanian, V., 2010. Exceptional events management applied to roller compaction of pharmaceutical powders. J. Pharm. Innov. 5, 147–160. https://doi.org/10.1007/s12247-010-9087-x

Hancock, B.C., Carlson, G.T., Ladipo, D.D., Langdon, B.A., Mullarney, M.P., 2002. Comparison of the mechanical properties of the crystalline and amorphous forms of a drug substance. Int. J. Pharm. 241, 73–85. https://doi.org/10.1016/S0378-5173(02)00133-3

Heckel, R.W., 1961. Density-Pressure Relationships in Powder Compaction. Trans. Metall. Soc. AIME 221, 671–675.

Hiestandx, E.N., Wells, J.E., Peot, C.B., Ochs, J.F., 1977. Physical processes of tableting. JPharmSci 66, 510–519.

Johanson, J.R., 1965. A Rolling Theory for Granular Solids. J. Appl. Mech. 32, 842. https://doi.org/10.1115/1.3627325

Johnson, W., Mellor, P.B., 1973. Engineering plasticity. London : Van Nostrand-Reinhold.

Kleinebudde, P., 2004. Roll compaction/dry granulation: Pharmaceutical applications. Eur. J. Pharm. Biopharm. 58, 317–326. https://doi.org/10.1016/j.ejpb.2004.04.014

KOPP, S., BEYER, C., GRAF, E., KUBEL, F., DOELKER, E., 1989. Methodology for a Better Evaluation of the Relation Between Mechanical Strength of Solids and Polymorphic Form. J. Pharm. Pharmacol. 41, 79–82. https://doi.org/10.1111/j.2042-7158.1989.tb06397.x

Lam, K., Newton, J., 1991. Investigation of applied compression on the adhesion of powders to a substrate surface 65, 167–175. https://doi.org/10.1016/0032-5910(91)80179-M

Miguélez-Morán, A.M., Wu, C.Y., Dong, H., Seville, J.P.K., 2009. Characterisation of density distributions in roller-compacted ribbons using micro-indentation and X-ray micro-computed tomography. Eur. J. Pharm. Biopharm. 72, 173–182. https://doi.org/10.1016/j.ejpb.2008.12.005

Omar, C.S., Dhenge, R.M., Osborne, J.D., Althaus, T.O., Palzer, S., Hounslow, M.J., Salman, A.D., 2015. Roller compaction: Effect of morphology and amorphous content of lactose powder on product quality. Int. J. Pharm. 496, 63–74. https://doi.org/10.1016/j.ijpharm.2015.06.032

Osborne, J., 2013. Bonding Mechanisms Involved in the Roller Compaction of an Amorphous Food Material. The Uniersity of Sheffield.

Patel, B.A., Adams, M.J., Turnbull, N., Bentham, A.C., Wu, C.Y., 2010. Predicting the pressure distribution during roll compaction from uniaxial compaction measurements. Chem. Eng. J. 164, 410–417.

https://doi.org/10.1016/j.cej.2009.12.022

Paul, S., Sun, C.C., 2017. Gaining insight into tablet capping tendency from compaction simulation. Int. J. Pharm. 524, 111–120. https://doi.org/10.1016/j.ijpharm.2017.03.073

Paul, S., Taylor, L.J., Murphy, B., Krzyzaniak, J., Dawson, N., Mullarney, M.P., Meenan, P., Sun, C.C., 2017. Mechanism and Kinetics of Punch Sticking of Pharmaceuticals. J. Pharm. Sci. 106, 151–158. https://doi.org/10.1016/j.xphs.2016.07.015

Podczeck, F., Newton, J.M., James, M.B., 1996. The influence of constant and changing relative humidity of the air on the autoadhesion force between pharmaceutical powder particles. Int. J. Pharm. 145, 221–229. https://doi.org/10.1016/S0378-5173(96)04774-6

Saniocki, I., 2014. New Insights into Tablet Sticking : Characterization and Quantification of Sticking to Punch Surfaces during Tablet Manufacture by Direct Compaction Dissertation.

Sonnergaard, J.M., 1999. A critical evaluation of the Heckel equation. Int. J. Pharm. 193, 63–71. https://doi.org/10.1016/S0378-5173(99)00319-1

Standard institution, B., 1977. Determination of flexural properties. Three point method, in: Methods of Testing Plastics. BSI.

Wu, C.Y., Hancock, B.C., Mills, A., Bentham, A.C., Best, S.M., Elliott, J.A., 2008. Numerical and experimental investigation of capping mechanisms during pharmaceutical tablet compaction. Powder Technol. 181, 121–129. https://doi.org/10.1016/j.powtec.2006.12.017

Wu, C.Y., Hung, W.L., Miguélez-Morán, A.M., Gururajan, B., Seville, J.P.K., 2010. Roller compaction of moist pharmaceutical powders. Int. J. Pharm. 391, 90–97. https://doi.org/10.1016/j.ijpharm.2010.02.022

Yusof, Y.A., Smith, A.C., Briscoe, B.J., 2005. Roll compaction of maize powder. Chem. Eng. Sci. 60, 3919–3931. https://doi.org/10.1016/j.ces.2005.02.025

Table 1. Particle size distribution (d10, d50, and d90) for the powder feeds together with their single particle yield strengths, true densities and amorphous contents.

Materials	d10 (μm)	d50 (μm)	d90 (μm)	Yield strength (MPa)	True density (Kg/m3)	Amorphous content (%)
CaCO3	5	23	87	435 ± 9	2930	~0 [a]
mannitol	12	40	138	233 ± 14	1514	~0 [b]

lactose 200M	9	35	82	200 ± 2	1545	2.67 [c]
anhydrous lactose	26.5	132	281	182 ± 3.5	1589	0.2 [d]
starch	14.8	54	138	123 ± 2.7	1449	34 [e]
maltodextrin	21.5	100	241	81 ± 2	1440	~100 [f]
MCC	23	49	104.5	69 ± 1	1594	15 [g]

[a] : Jones, 2017; Moore, n.d. [b] : Cornel et al., 2010; Development and Pharmacy, 1987, [b] and [c] : Omar et al., 2015 , [e] : Rangelov et al., 2017, [f] : Thorat et al., 2017, [g] : Ahvenainen et al., 2016; Awa et al., 2015; Vieira and Pasquini, 2014

Table 2. Compressibility factor and flow properties of the materials.

Material	$(\delta_E)°$	$(\emptyset_w)°$ Smooth coupon	$(\emptyset_w)°$ knurled coupon	κ
CaCO3	44.8 ± 0.3	17.1 ± 0.5	34.4 ± 0.2	13.2 ± 0.7
mannitol	39.3 ± 0.1	10.3 ± 0.7	31.5 ± 0.1	10.3 ± 0.2
lactose 200M	46.3 ± 0.3	16.8 ± 1.1	34.5 ± 0.4	12.7 ± 0.6
anhydrous lactose	40.6 ± 0.2	13.6 ± 1.1	32.1 ± 0.1	8.8 ± 0.1
starch	34.2 ± 0.1	9.5 ± 1.9	27.7 ± 0.1	8.4 ± 0.3
maltodextrin	40 ± 0.1	10.2 ± 1.1	31.1 ± 0.3	6 ± 0.3
MCC	44.5 ± 0.2	6.9 ± 0.3	35.1 ± 0.2	5.3 ± 0.9

Table 3. Effect of the maximum roll stress on the splitting and sticking behaviour of the ribbons formed from unlubricated (a) smooth and (b) knurled rollers. Grey dotted areas indicate a non-achievable condition. Red regions indicate the occurrence of splitting/sticking. Green regions indicate the non-occurrence of splitting/sticking. Spitting is designated by T (transversal splitting), Ln (longitudinal splitting into n pieces) and LJ (longitudinally joined splitting).

(b)

Figure showing Maximum stress (MPa) ranges for CaCO₃, mannitol, lactose 200M, anhydrous lactose, starch, maltodextrin, and MCC under Split and Stick conditions, with axis markings at 50, 100, 150, 200, 250, 300, 350, 400, 450, 500, 550, 600, 650, 700 MPa. Vertical labels read "Outside roller compactor stress range."
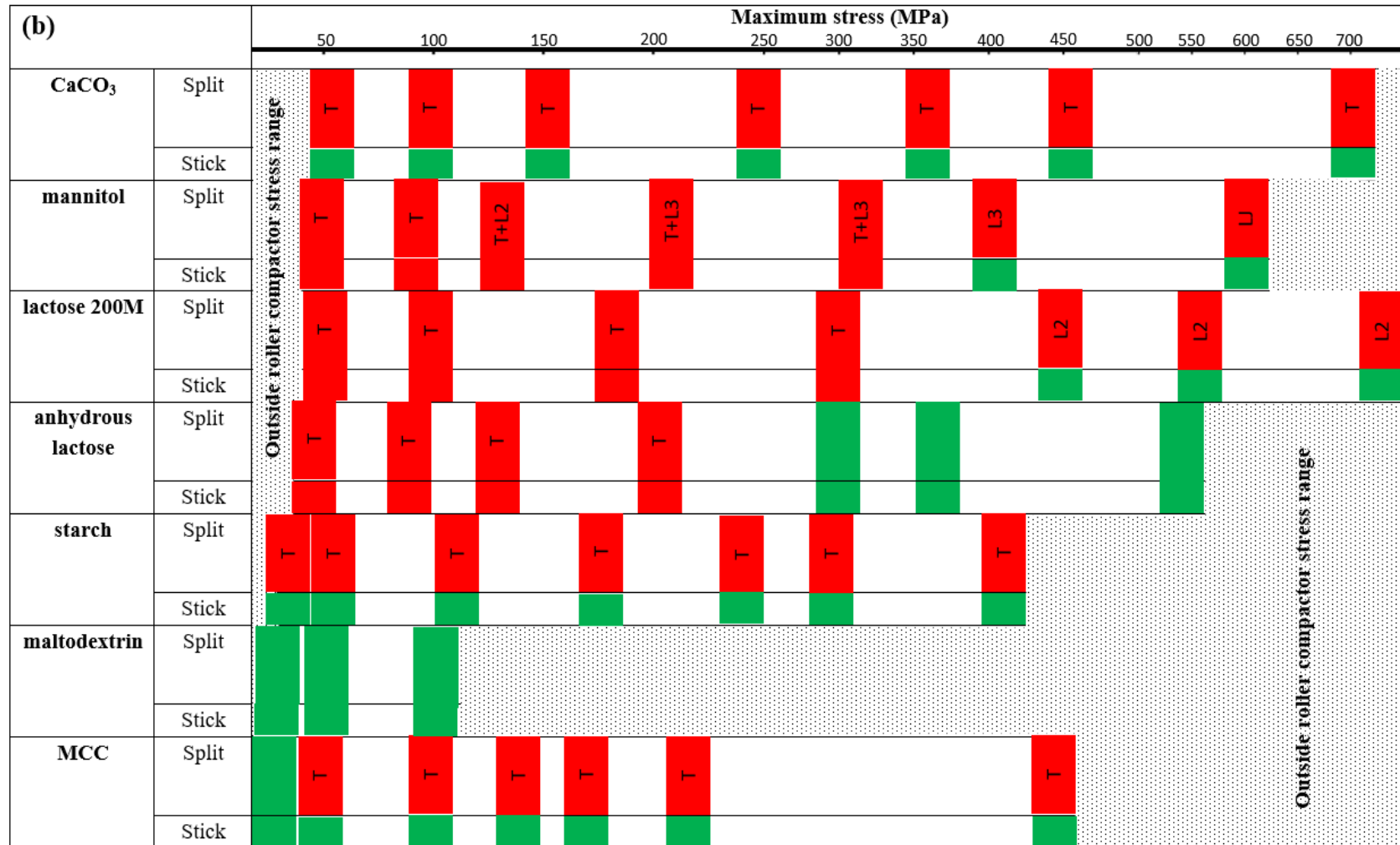
Table A1. The relationship between roller separating force and hydraulic pressure as given by the

manufacturer (Alexanderwerk) (Al-Asady et al., 2015).

Hydraulic pressure (MPa)	Roller separating force (kN)
1.8	7.46
3	12.43
5	20.72
80	33.15
12	49.76
15	62.16
23	95.38

(a)   (b)
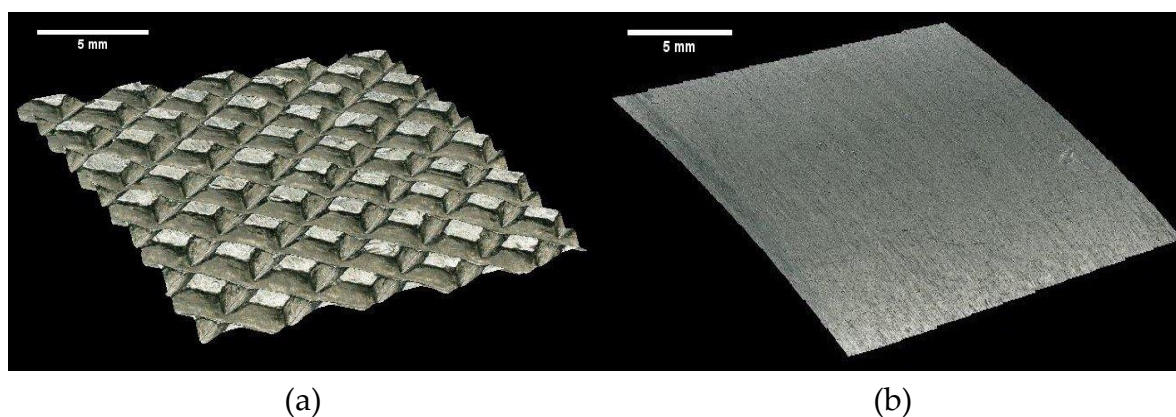
Figure 1. Optical image of a section of the knurled roller surface (a) and the smooth roller surface (b).
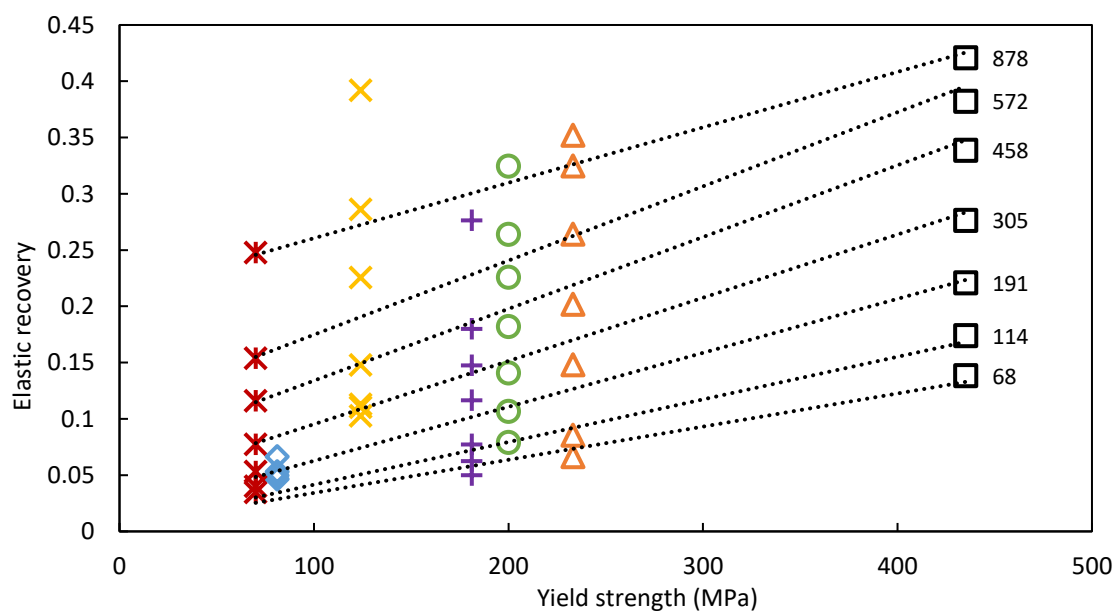
Figure 2. The elastic recovery of tablets measured during uniaxial compaction as a function of the single particle yield strength for the range of compressive stresses (MPa) investigated as given to the right of each data set; the lines are to guide the eye. The symbols for the powder feeds correspond to: CaCO3 (□), mannitol (△), lactose 200M (○), anhydrous lactose (+), starch (x), maltodextrin (◇) and MCC (✳).
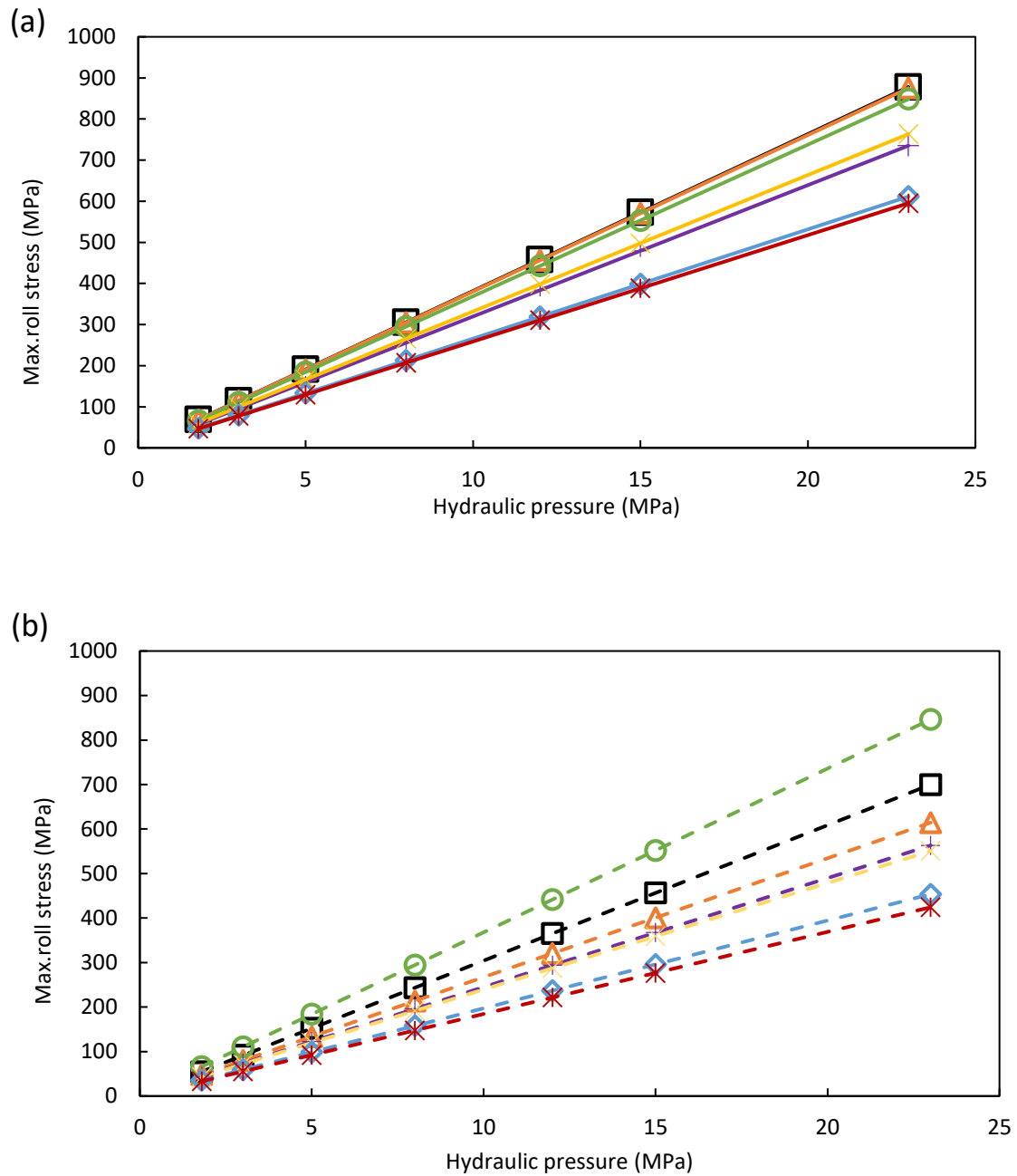
Figure 3. Maximum roll stress as a function of the hydraulic pressure for the (a) smooth and (b) knurled rollers and the following feed powders: CaCO3 (□), mannitol (△), lactose 200M (○), anhydrous lactose (+), starch (x), maltodextrin (◇) and MCC (✱).
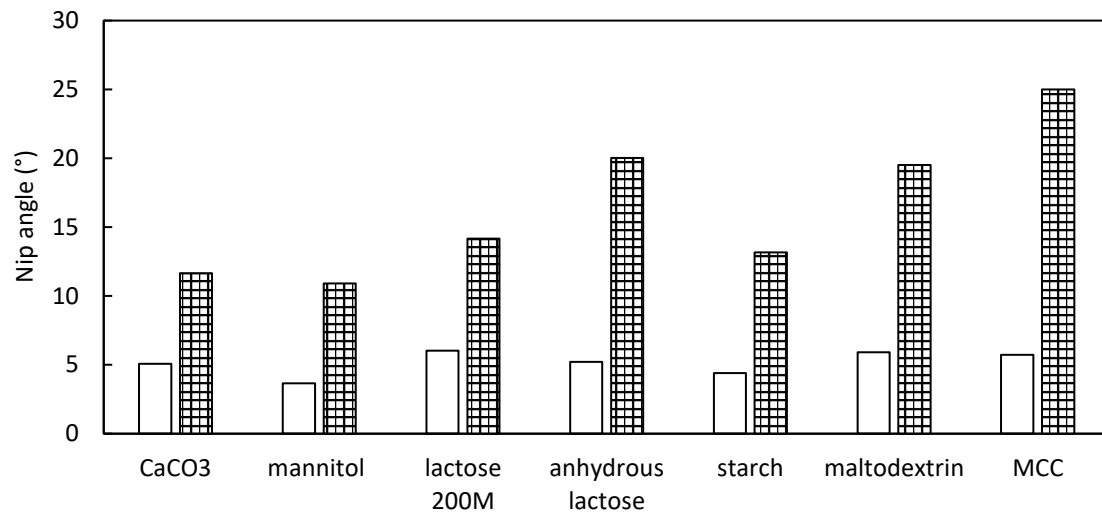
Figure 4. The calculated nip angles for the different types of powder feed materials, which were compacted using knurled (▣) and smooth (▢) rollers.
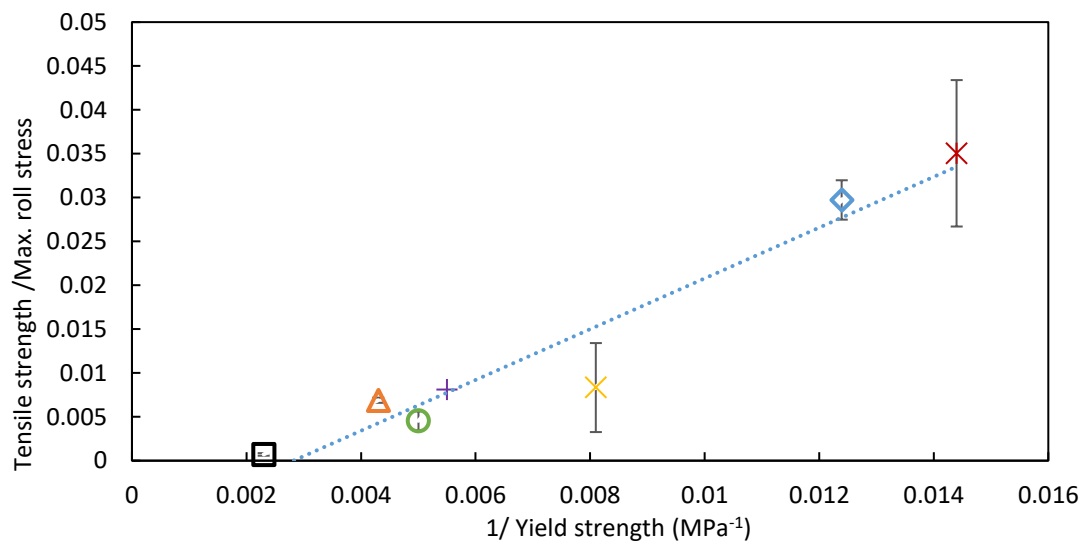
Figure 5. The mean ratio of the tensile strength and the maximum roll stress as a function of the reciprocal of the yield strength for CaCO3 (▢), mannitol (△), lactose 200M (◯), anhydrous lactose (+), starch (✕), maltodextrin (◇) and MCC (✳); the line is the best linear fit (Eq. (4)).
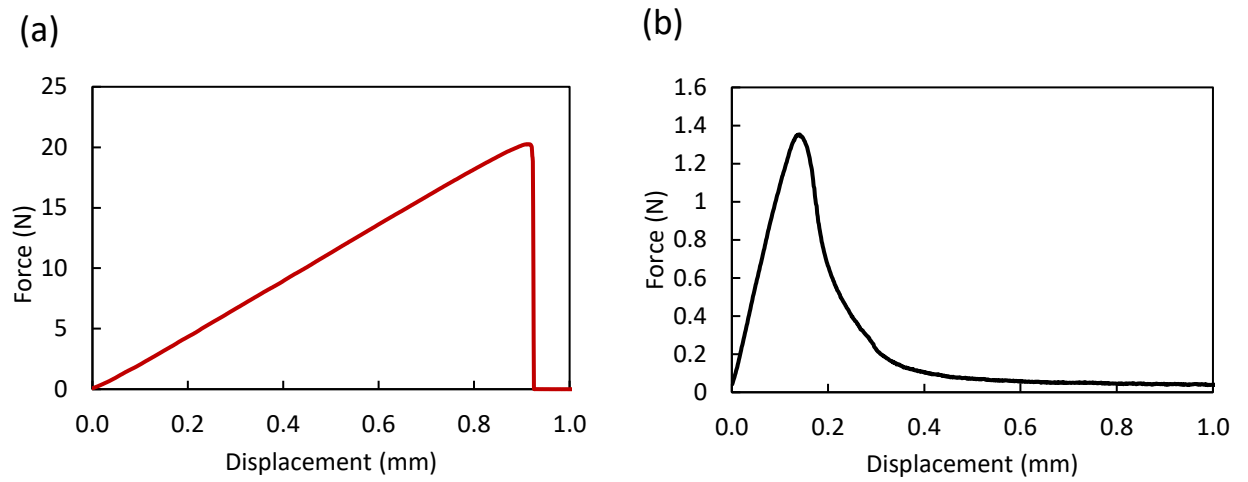
Figure 6. The applied force as a function of the displacement for three-point fracture measurements: (a) the unstable fracture of MCC and (b) the stable fracture of CaCO3 ribbons made at maximum roll stresses of 595 and 878 MPa respectively. The ribbons formed from all the powder feeds except those from CaCO3 exhibited unstable fracture at all maximum roll stresses.

(a)   (b)
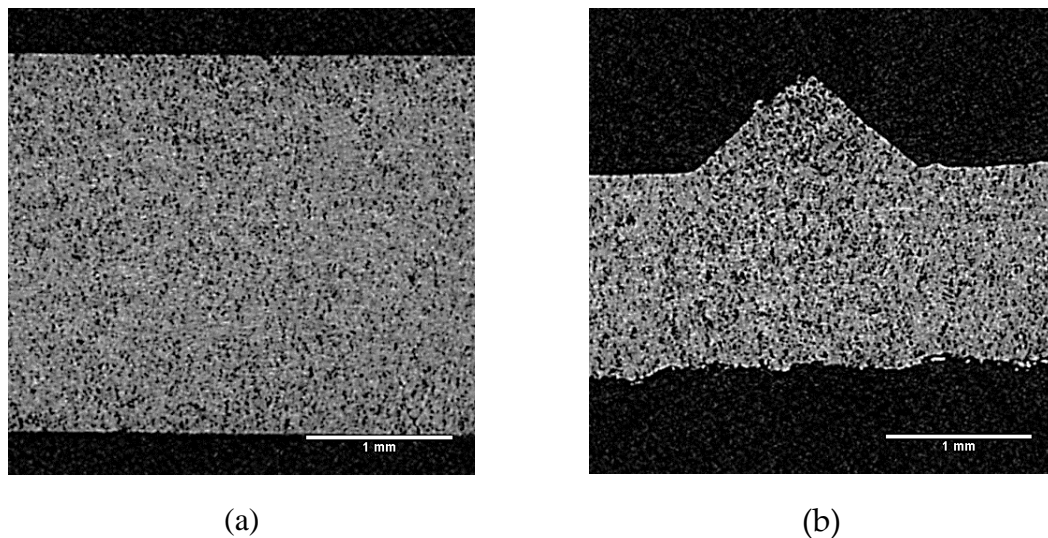
Figure 7. X-ray tomography images of MCC ribbons made with the (a) smooth and (b) knurled rollers at maximum roll stresses of 129 and 92 MPa respectively, corresponding to a hydraulic pressure of 5 MPa.

69 MPa No longitudinal splitting	114 MPa L2	304 MPa L3	571 MPa LJ
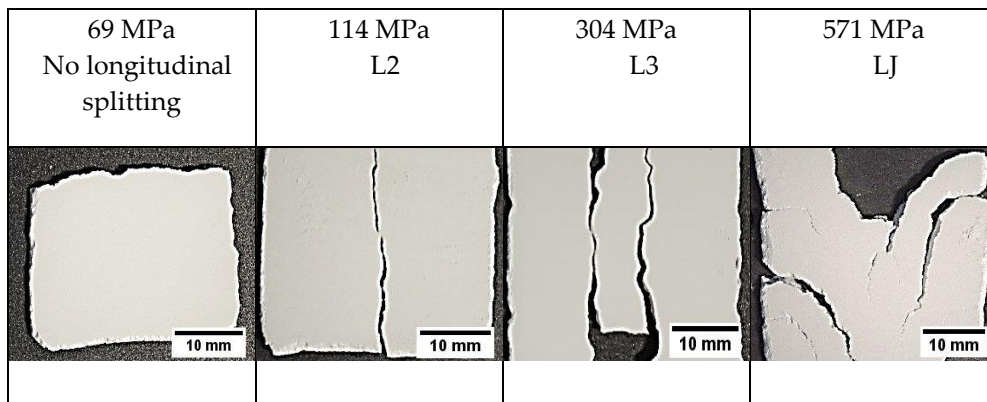
Figure 8. Images of mannitol C160 ribbons that are produced at different maximum roll stresses.
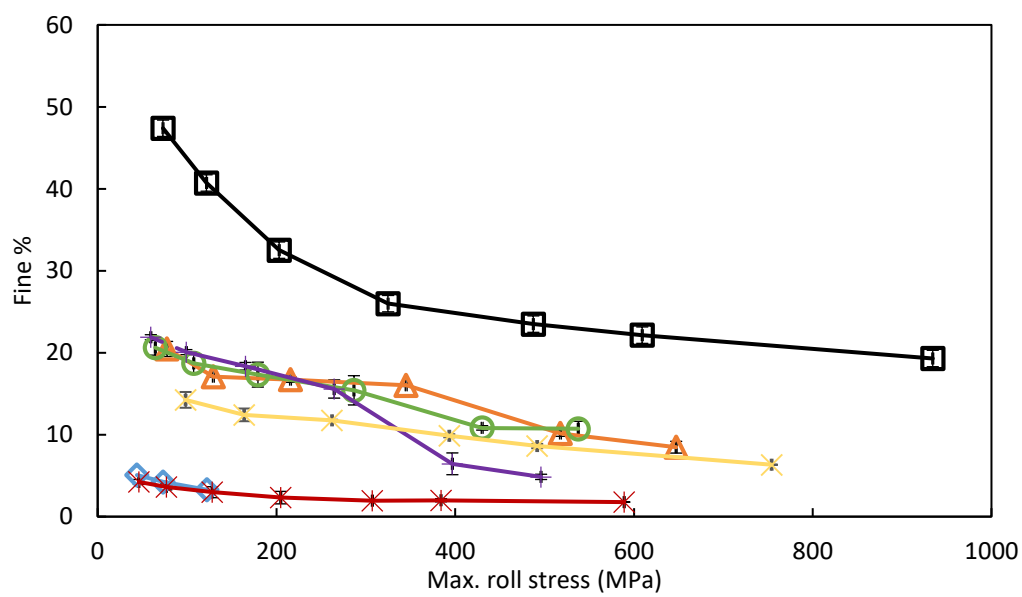
Figure 9. The amount of fines (w/w%) produced for the powder feeds with the unlubricated smooth rollers as a function of the maximum roll stress. The symbols for the powder feeds correspond to: CaCO3 (□), mannitol (△), lactose 200M (○), anhydrous lactose (+), starch (x), maltodextrin (◇) and MCC (✳).
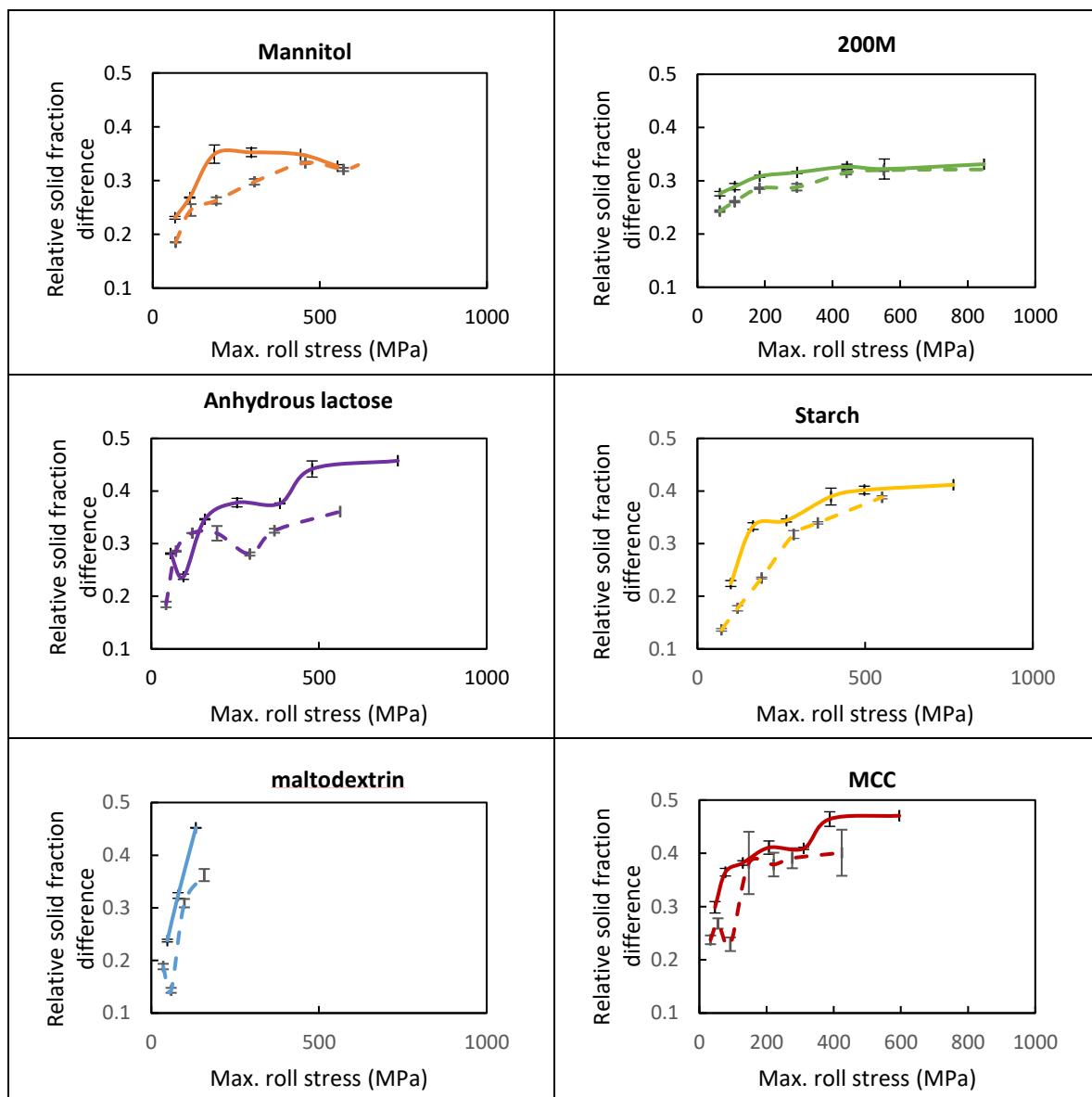
Figure 10. The relative solid fraction difference across the ribbons (Eq. (3)) as a function of the maximum roll stress for the ribbons formed with the unlubricated (solid lines) smooth and (dashed lines) knurled rollers. The CaCO3 ribbons were excluded since it exhibited anomalous splitting behaviour.
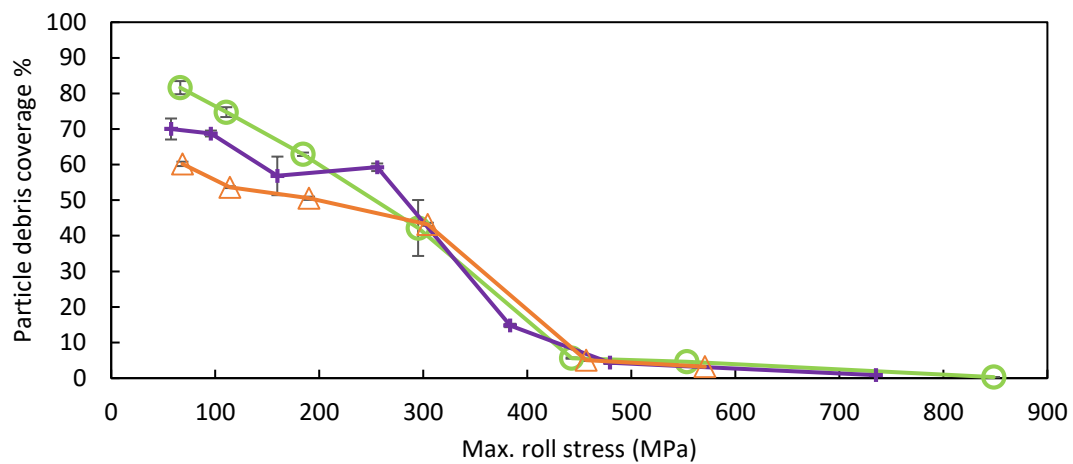
Figure 11. The particle debris coverage on the smooth unlubricated rollers measured after the scrapers as a function of the maximum roll stress for the mannitol (△), lactose 200M (○), and anhydrous lactose (+). Adhesion was absent for starch, MCC and CaCO3.
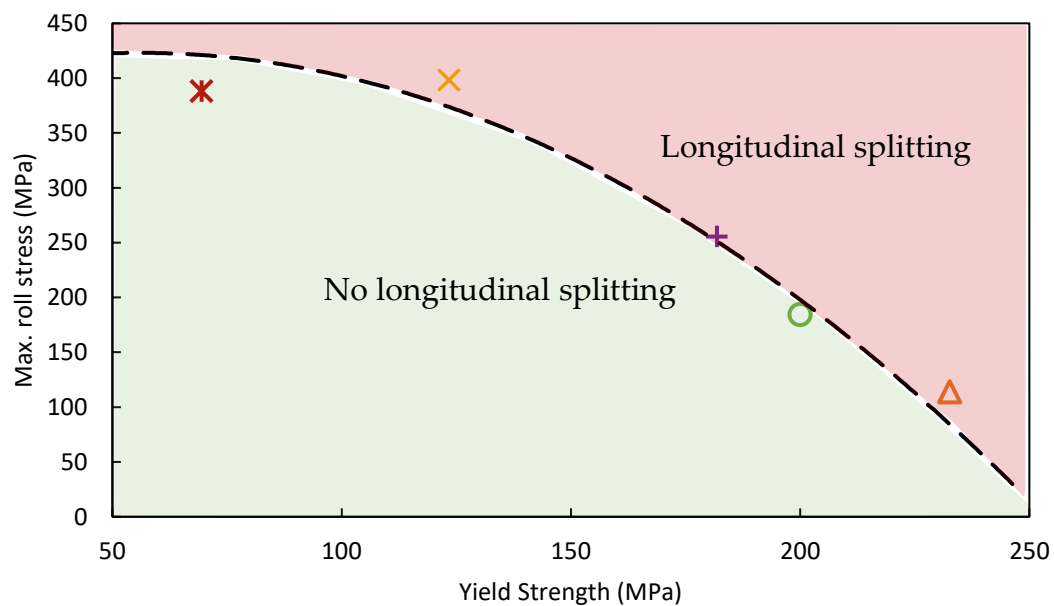
Figure 12. A map of the transition from no splitting to longitudinal splitting in coordinates of the maximum roll stress and the single particle yield strength for the unlubricated and externally lubricated smooth rollers. The symbols for the powder feeds correspond to: mannitol (△), lactose 200M (○), anhydrous lactose (+), starch (x), maltodextrin (◇) and MCC (✳). Longitudinal splitting was not observed for CaCO3.
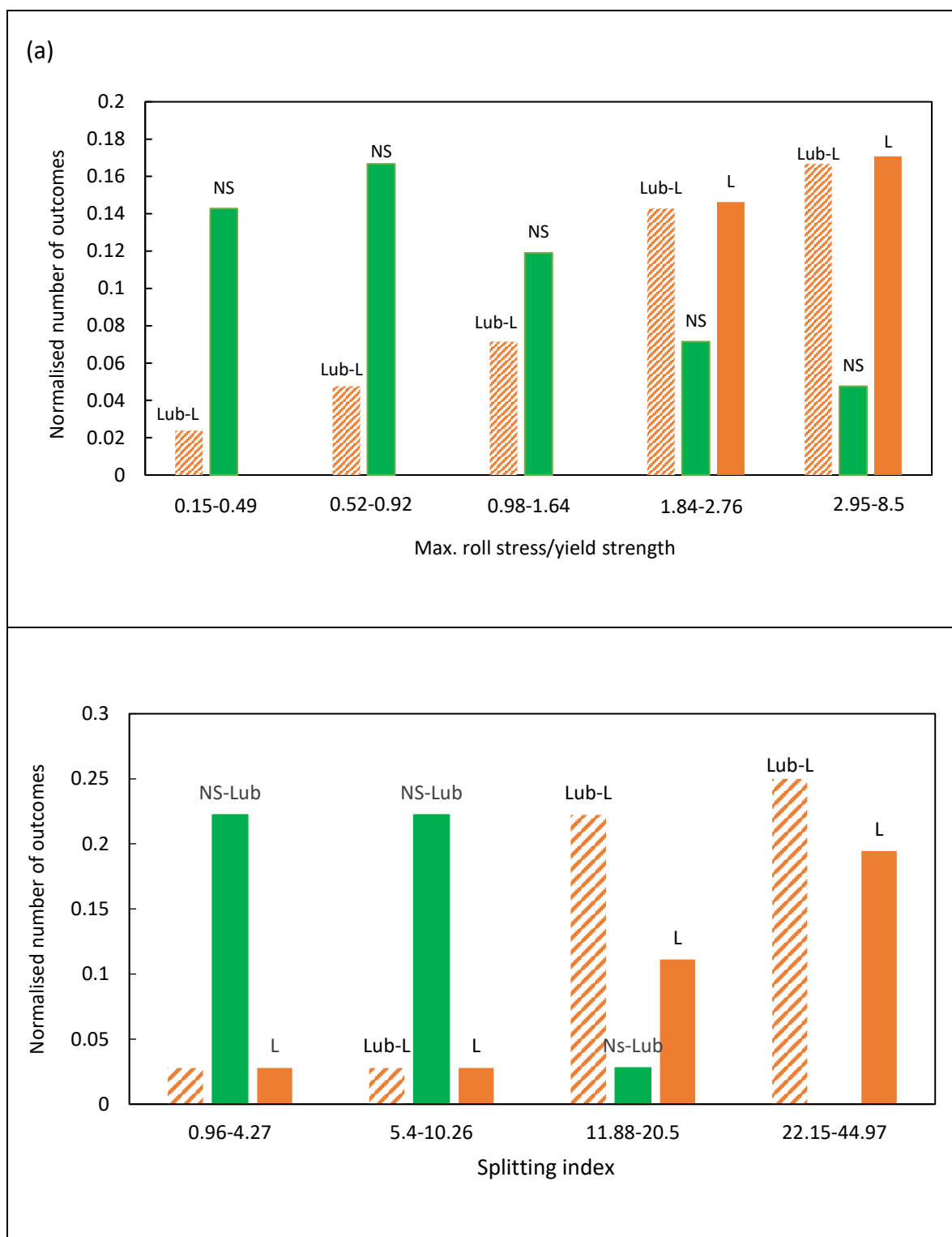
Figure 13. A histogram of the number of non-splitting (■) and longitudinal splitting outcomes per powder feed normalised by the total number of outcomes that were observed with the unlubricated (■) and lubricated smooth rollers (▨) based on (a) the ratio of the maximum roll stress and single particle yield strength and (b) the splitting index. In the case of the externally lubricated rollers, all the powders feeds except for CaCO3 exhibited pure longitudinal splitting (without adhesion or transverse splitting) at stresses greater than some minimum value. For the unlubricated rollers, longitudinal splitting was only observed at greater stresses. NS refers to no splitting, L to longitudinal splitting and LUB to external roller lubrication.
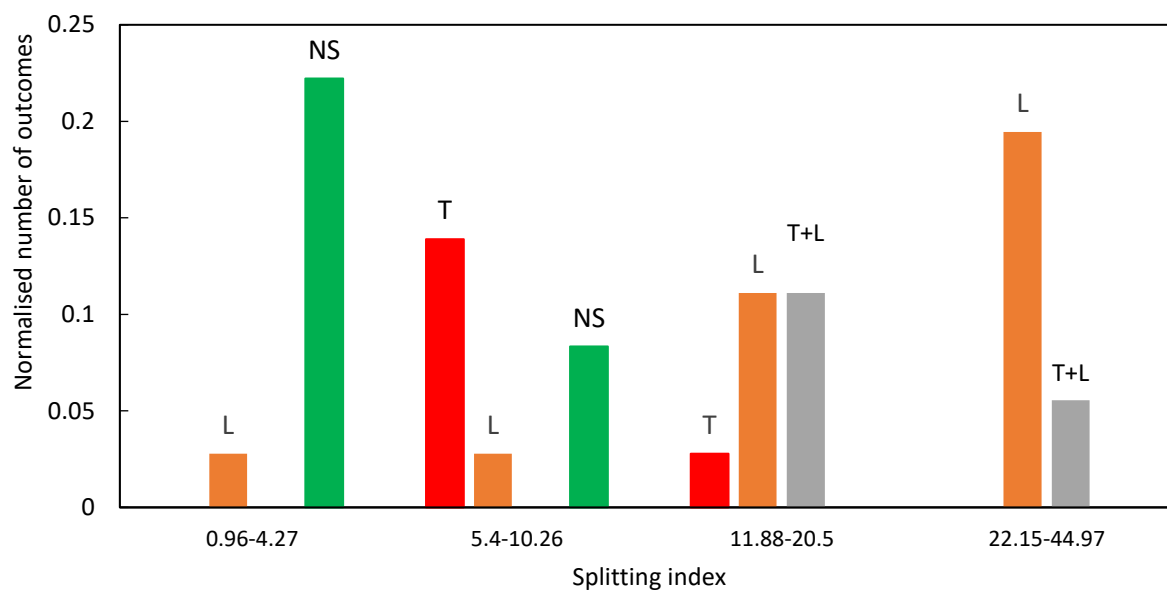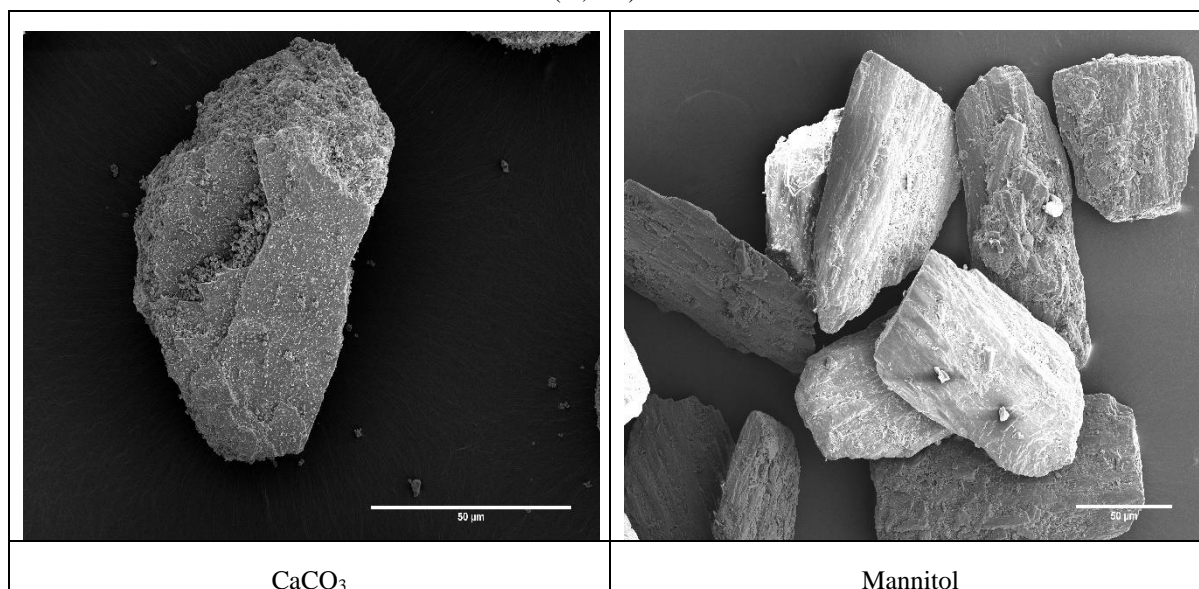
Figure 14. A histogram based on the splitting index of the number of non-splitting and splitting outcomes per powder feed normalised by the total number of outcomes that were observed with the unlubricated smooth rollers. The data for CaCO3 ribbons are not included since its splitting behaviour is anomalous. The coding refers to transversal (■, T), longitudinal (■, L), mixed transversal-longitudinal (■, T+L) and no splitting (■, NS).
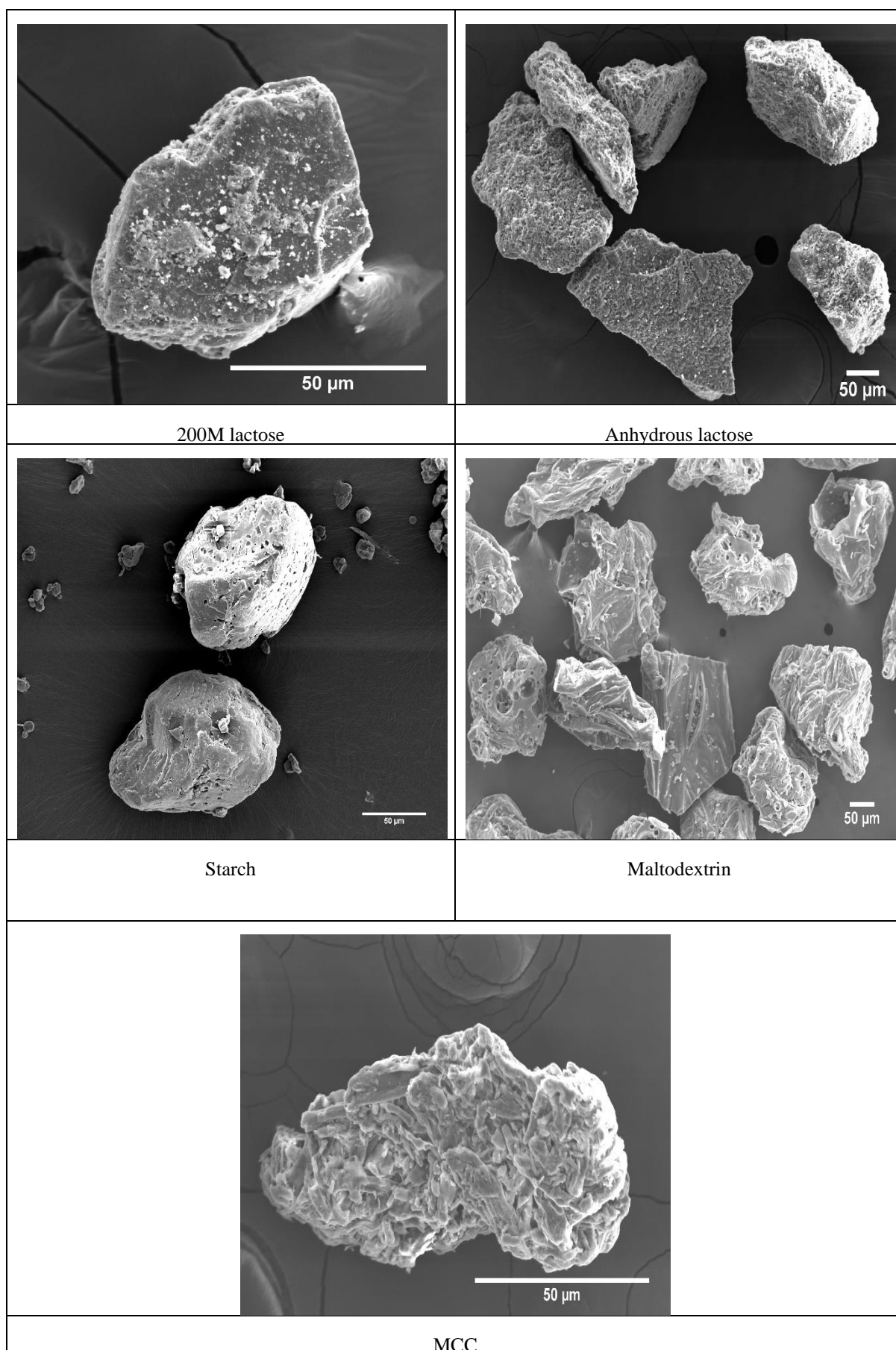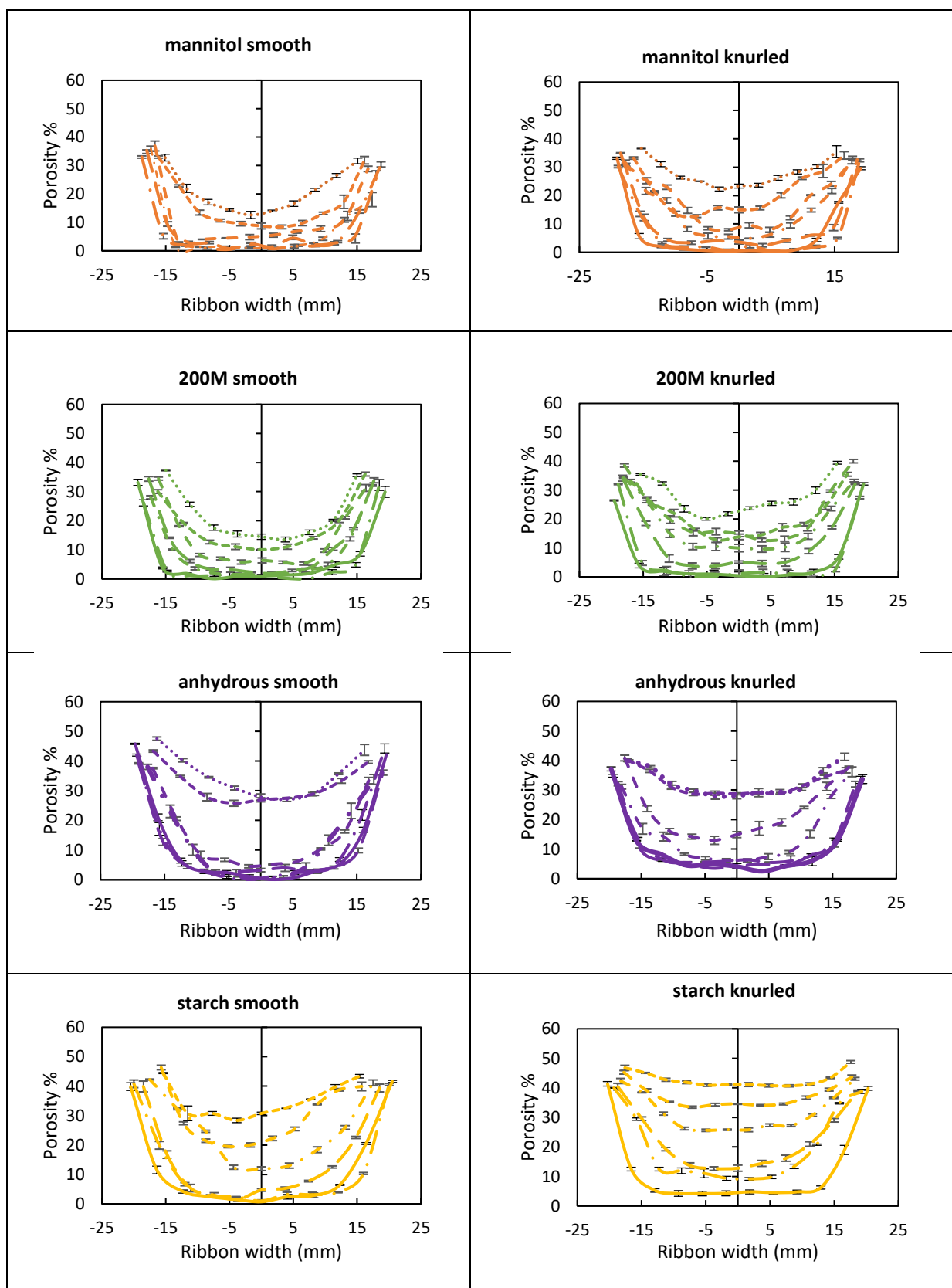

| CaCO$_3$ | Mannitol |

Figure A1. Scanning electron microscopy images of all powders used in this study.

mannitol smooth

mannitol knurled

200M smooth

200M knurled

anhydrous smooth

anhydrous knurled

starch smooth

starch knurled

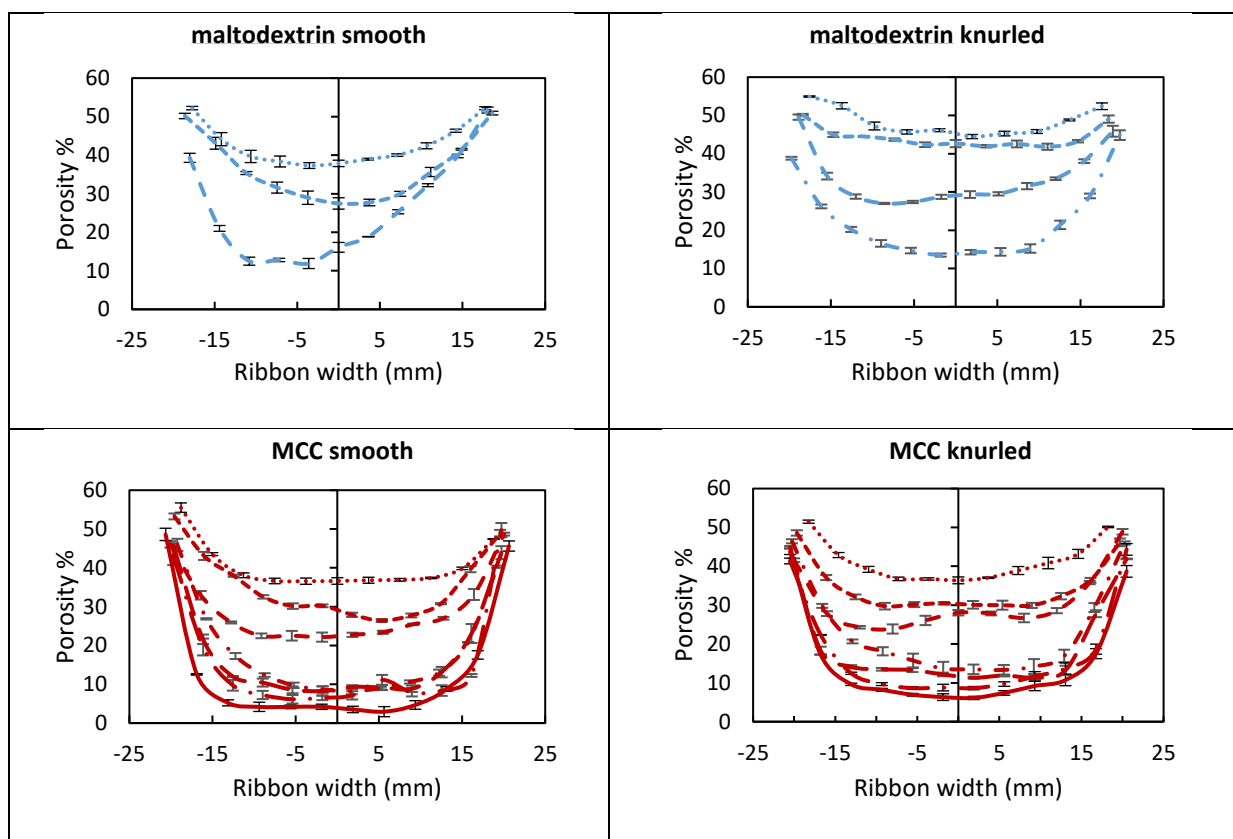Figure A2: The porosity profile across ribbon width calculated from the X-ray data for the ribbons produced from all powder feed except CaCO₃. The profiles are for the ribbons produced using smooth rollers (left column) and knurled rollers (right column). (…. 18 bar, ---- 30 bar, – – –50 bar, - · - 80 bar, —— —120bar, —·— 150 bar, and — 230 bar).

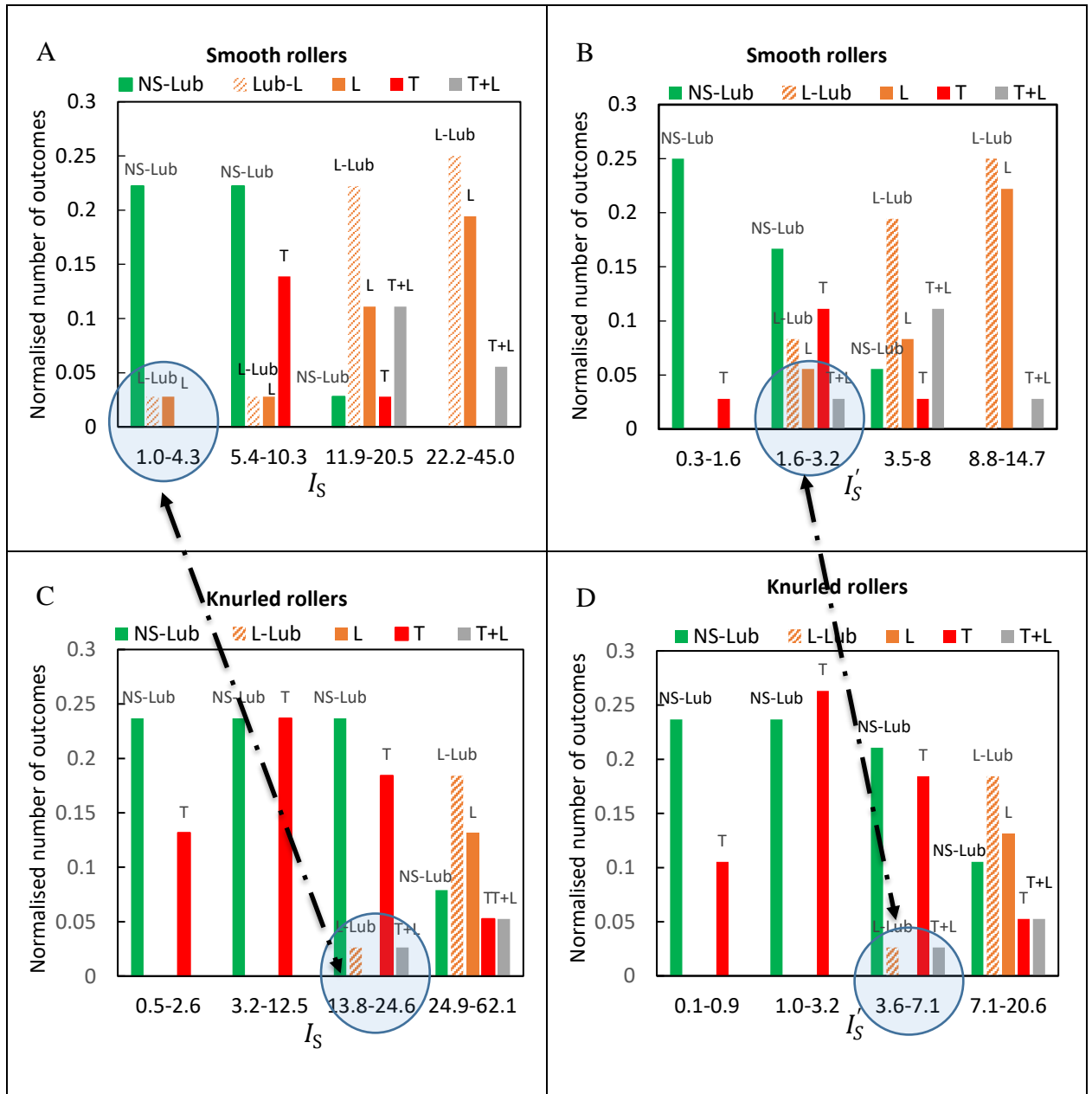Figure A3: A histogram based on the splitting index (I_S) and modified splitting index (I_S') of the number of non-splitting and splitting outcomes per powder feed normalised by the total number of outcomes that were observed with the unlubricated and lubricated smooth and knurled rollers. The data for CaCO$_3$ ribbons are not included since its splitting behaviour is anomalous. The coding refers to transversal (■, T), longitudinal (■, L), lubricated longitudinal (▨, L-Lub), mixed transversal-longitudinal (■, T+L) and no splitting (■, NS).